IJST (2014) 38A3: 243-252
Iranian Journal of Science & Technology

http://ijsts.shirazu.ac.ir

An unusual assemblage of talc-phengite-chlorite-K-feldspar in quartz schists from the Nahavand area, Sanandaj-Sirjan zone, Iran

J. Izadyar*, S. Mojab, O. Kuroshi and M. Zare

Department of Geology, University of Zanjan, University Blvd., Zanjan, Iran
E-mail: izadyar@znu.ac.ir

Abstract

For the first time, an unusual assemblage of talc-phengite-chlorite-K-feldspar was found in quartz schists from the Sanandaj-Sirjan zone in the Nahavand area in western Iran. The talc-bearing quartz schists occur as small bodies or lenses within pelitic schist layers and contain talc, phengite, chlorite, K-feldspar and quartz as major mineral constituents with subordinate amounts of calcite and graphite. Textural analysis revealed that talc, phengite, chlorite and K-feldspar are in sharp contact and no reaction rims between them were observed. Constructed petrogenetic gird in the K_2O-FeO-MgO-Al_2O_3-SiO_2-H_2O (KFMASH) model system containing talc, phengite, chlorite, K-feldspar, phlogopite and kyanite with excess quartz and H_2O shows that divariant assemblage of talc-phengite-chlorite-K-feldspar is stable over a wide P-T range defined by the following two univariant reactions: phengite + talc + quartz = chlorite + K-feldspar + kyanite + H_2O and chlorite + phlogopite + quartz = talc + phengite + K-feldspar + H_2O. Constructed Al_2O_3-$KAlO_2$-MgO+FeO (AKM) compatibility diagrams predict that phengite (X_{Ph} = 0.280, Y_{Ph} = 0.860), chlorite (X_{Chl} = 0.570, Y_{Chl} = 0.640), talc (X_{Tlc} = 0.160, Y_{Tlc} = 0.02) and K-feldspar are stable at P = 11 kbar and T = 400°C. This relatively high-pressure assemblage could be formed during the subduction of the Neo-Tethys oceanic plate under Iranian microcontinent.

Keywords: High-pressure metamorphism; Nahavand; Sanandaj-Sirjan zone; Talc-phengite-K-felds parassemblage

1. Introduction

In natural rocks, talc-phengite assemblage was first found in the piemontite-quartz schist in Serbia (Abraham and Schreyer, 1976). Abraham and Schreyer (1976) suggested that talc-phengite assemblage is an indicator of high-pressure metamorphism based on theoretical grounds in the K_2O-MgO-Al_2O_3-SiO_2-H_2O (KMASH) model system, although they also proposed an alternative hypothesis that this pair could be formed due to the presence of small amounts of additional non-KMASH components such as Fe_2O_3-MnO-CuO-NiO in phyllosilicates under low-pressure conditions. Massonne and Schreyer (1989) assessed the stability field of talc-phengite assemblage by the synthetic work in the KMASH model system containing kyanite, chlorite, talc, phlogopite and muscovite with excess quartz and H_2O. They proposed that the following two reactions: chlorite+ phlogopite + quartz = talc + muscovite + H_2O and talc + muscovite = phlogopite + quartz + H_2O intersect at an invariant point at 10.8 kbar and 610°C, which supported hypothesis 2 of Abraham and Schreyer (1976) regarding the high-pressure origin for talc-phengite assemblages. This assemblage was subsequently recognized in the western Alps (Chopin, 1981) and thereafter in a number of areas around the world in high-pressure metamorphic terrains such as the Sanbagawa metamorphic belt, Japan (Izadyar et al., 2000; Hatanaka and Hirajima, 1999; Ubukawa et al., 2007). Talc-kyanite and talc-omphacite assemblages have also been identified from ultra high-pressure metamorphic rocks (Reinecke, 1991; Mattinson et al., 2004; Liou and Zhang, 1995). However, the natural parageneses of talc-phengite and talc-kyanite usually coexist with Fe-bearing mineral phases such as garnet, biotite, chloritoid and chlorite (Chopin, 1981; Frank et al., 1987) and do not belong to the constituents of the simple KMASH model system. Wei and Powell (2003) calculated the KFMASH model system for high-pressure metapelites with mineral phases of garnet, chloritoid, chlorite, biotite, carpholite, talc, staurolite, kyanite with phengite, quartz/coesite and H_2O in excess. They documented the typical parageneses of talc-phengite and talc-kyanite for a variety of bulk compositions from several high-pressure terrains. Wei and Powell (2004) also calculated the stable mineral assemblages of Na-bearing metapelites in high-pressure conditions as

*Corresponding author
Received: 4 February 2013 / Accepted: 7 May 2014

they also occur widely in high-pressure metamorphic terrains (Chopin, 1981; Izadyar et al., 2000; Meyre et al., 1999; Theye et al., 1992). By using Schreinemakers' analyses and thermodynamic calculation based on the dataset of Holland and Powell (1998), Izadyar et al. (2000) indicated that the talc-phengite-albite assemblage from piemontite-quartz schists of the Sanbagwa metamorphic belt is stable at 580-600°C and 11.6-12 kbar. However, Ubukawa et al. (2007) obtained temperatures of 565-580°C and pressures of 9.5-10 kbar for talc-phengite assemblage in NCKFe^{3+}MASH model system in talc-Na pyroxene piemontite-quartz schist in the Sanbagawa metamorphic belt. None of these studies, either experimental or calculated, have addressed a talc-phengite-K-feldspar assemblage. In fact, only Massonne and Schreyer (1989) proposed high-pressure stability field for the talc-phengite-K-feldspar assemblage purely on theoretical grounds but it is not reported in natural rocks from high-pressure metamorphic terrains. During a petrological investigation in the Nahavand area of the Sanandaj-Sirjan zone, an unusual assemblage of talc-phengite-chlorite-K-feldspar was recognized in quartz schists. This paper is the first to describe this assemblage, to characterize its mineralogy and texture and to explain its equilibrium condition based on the petrogenetic grid in the KFMASH model system containing K-feldspar.

2. Geological setting

The Sanandaj-Sirjan zone, which is 1500km long and up to 200km wide, stretches from the northwest to the southwest of Iran and is located between the central Iran block and Zagros Fold-thrust belt (Stoclin, 1968; Berberian and King, 1981; Alavi, 1994) (Fig. 1A). The Sanandaj-Sirjan zone consists of mafic-ultramafic rocks, metamorphic complexes and Paleozoic-Mesozoic sequences that underwent amphibolite/greenshist-facies metamorphism during the Cretaceous-Tertiary continental collision between the Afro-Arabian continent and the Iranian microcontinent (Sengör and Natalin, 1996; Mohajjel and Fergusson, 2000; Mohajjel et al., 2003). From the southwest to the northeast it consists of several elongated sub-zones (Fig. 1B): (1) a radiolarite sub-zone consisting of Triassic-Cretaceous shallow marine limestone and dominant deep-marine radiolarite; (2) a Bisotun sub-zone that includes Late Triassic to Late Cretaceous limestone; (3) an ophiolite sub-zone that is the location of the Zagros suture zone; (4) a marginal sub-zone that contains abundant Late Jurassic-Early Cretaceous volcanic rocks in addition to shallow marine strata in the Cretaceous unit and (5) a complexly deformed sub-zone (Mohajjel et al., 2003). The last sub-zone is distinguished from the other sub-zones by abundant metamorphic rocks. The main rock types of the complexly deformed sub-zone are schist, marble, amphibolite, quartzite, dolomite-marble and metasandstone. All sub-zones are imbricated in a complicated thrust system with out-of-sequnce thrusts that locally juxtaposes the younger units over the older ones (Mohajjel et al., 2003). The Nahavand area belongs to the complexly deformed sub-zone and is located near the main Zagros reverse fault, which is proposed as a suture zone between the Arabian plate and Eurasia (Sengör, 1984; Agard et al., 2006; Ghasemi and Talbot, 2006) (Fig. 1B). Apart from a thin ophiolite unit, the lithologic units in the Nahavand region can be generally subdivided into two groups of metamorphosed and non-metamorphosed rocks (Alavi and Mahdavi, 1994) (Fig. 2). The metamorphic rocks include five different successions that are in fault contact with both the overlying and underlying rocks. The oldest one (PTrm) is a sequence of massive marbles of Permian-Triassic age that are strongly sheared and mylonitized near the contact with the underlying rocks. The next succession (TrJmv) consists of an assemblage of Middle to Upper Triassic-Lowermost Jurassic metamorphosed basaltic and andesite-basaltic lava flows (with tholeitic affinities). This assemblage contains locally occurring pillow structures interlayered with well-foliated marbles that have thin, upward increasing slate layers. Small plutons of gabbro and diorite (now metamorphosed) have locally intruded this assemblage (Alavi and Mahdavi, 1994) (Fig. 2). The third unit (TrJm) consists entirely of a sequence of fossiliferous marbles of Late Triassic to Early Jurassic. The fourth succession (Jsv) is a sequence of Lower Jurassic slates, phyllites and metagreywakes that have intercalations of marbles and metamorphosed volcanic rocks in the lower parts. The fifth lithological unit (Jh) consists of an Upper Liassic succession of cordierite-bearing hornfels which is the product of contact metamorphism due to the intrusion of Late Cretaceous granitoid plutons (Alavi and Mahdavi, 1994) (Fig. 2).

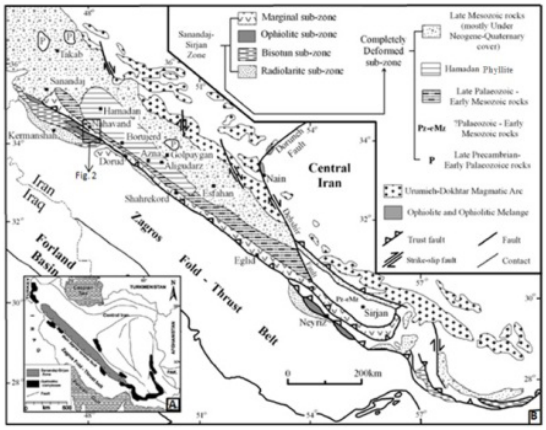

Fig. 1. (A) Simplified structural map of Iran showing the location of the Sanandaj-Sirjan zone. (B) Tectonic map of southwestern Iran showing the divisions of the Sanandaj-Sirjan zone (modified after Mohajjel et al., 2003)

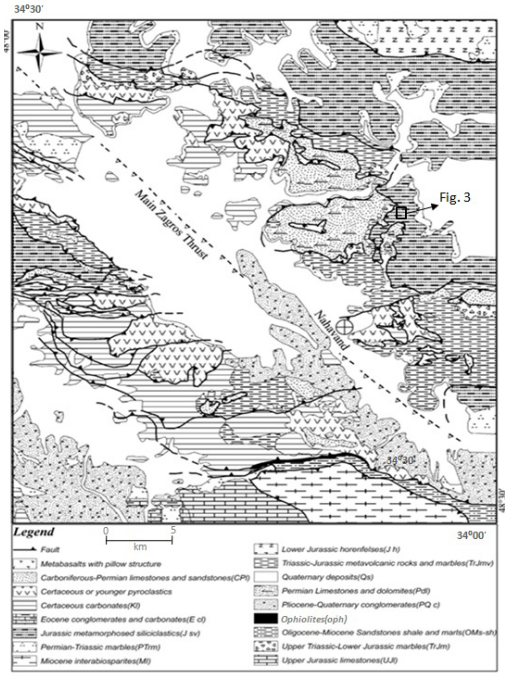

Fig. 2. Geological map of the Nahavand area (modified after Alavi and Mahdavi, 1994)

3. Petrography

Quartz schists were collected from the Jsv unit that is a Lower Jurassic sequence mostly of pelite and greywake origins (Fig. 3). This sequence usually occurs in the northwest of the Nahavand region. The quartz schists form 30-50 m thick layers interbedded with 10-30 m thick marbles and 100-150 m thick pelitic schists. They also occur as small bodies or lenses from one centimeter up to a maximum of three meters within pelitic schist layers. An unusual but stable mineral assemblage of talc-phengite-chlorite-K-feldspar could only be found in the quartz schist occurring as small bodies or lenses within pelitic schists. Therefore, based on the field and mineral assemblages, two types of quartz schists are recognized in the studied area which are named talc-free and talc-bearing quartz schists (Fig. 3). The mineral parageneses of these two quartz schists are tabulated in Table 1. The talc-bearing quartz schist contains coarser grains than talc-free quartz schist and commonly shows compositional banding of quartz-rich and mica-rich bands. The width of the quartz-rich bands ranges from 1 to 2 mm, and they are mainly composed of quartz, K-feldspar and subordinate amounts of phengite and chlorite. The mica-rich bands mostly contain phengite, talc and chlorite with minor amounts of quartz and K-feldspar. The width of these bands ranges from 1 to 2 mm. The textural relationship clearly shows that talc and phengite are in sharp contact, and no reaction rims between them are observed (Figs. 4A, 4B, 4D and 4E). Chlorite is one of the major constituent minerals in both talc-bearing and talc-free quartz schists. It occurs in quartz-rich and mica-rich bands in sharp contact with talc, phengite and K-feldspar in talc-bearing assemblage (Figs. 4C and 4F) and with muscovite in talc-free assemblage. It is hard to distinguish talc from phengite under the microscope, because talc has similar birefringence to that of phengite. However, talc can be distinguished from phengite by its lower interference colour under microscope, because talc's lower Mohs hardness (H = 1) should enhance the thinning during thin-section making rather than surrounding harder minerals, such as quartz (H = 7) and phengite (H = 2.5-3)(Figs 4A and 4B). Talc occurs only in talc-bearing quartz schists in sharp contact with phengite, chlorite and K-feldspar (Figs. 4A, 4B, 4C, 4D, 4E and 4F). K-feldspar occurs in both talc-bearing and talc-free quartz schists and also in both mica-rich and quartz-rich bands (Fig. 4A and 4C). Usually it shows an elongated form but sometimes in the talc-free samples a sigmoidal form is seen with asymmetrical pressure shadows. Calcite and graphite are not common, but are present in the matrix of both talc-bearing and talc-free quartz schists.

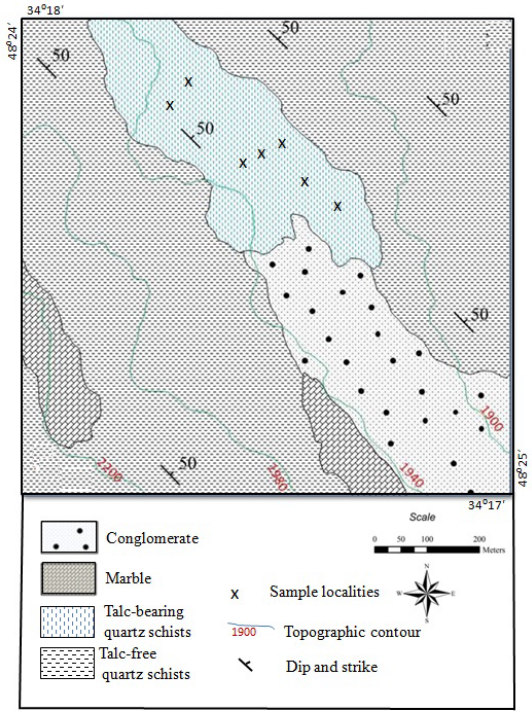

Fig. 3. Lithological map of the studied area and sample localities

Table 1. Mineral assemblages of talc-bearing and talc-free quartz schists from the Nahavand area

Mineral Na.	Chl	Ms	Ph	Tlc	Kfs	Qz	Cal	Gr
C18	+	+	+	+	+	+	+	-
C19	+	+	-	-	-	+	+	+
C20	+	-	+	+	+	+	-	+
C21	+	+	+	+	+	+	-	-
C22	+	+	+	+	+	+	+	-
C44	+	-	+	-	+	+	+	+
C32	+	+	-	-	-	+	+	+
C53	+	+	-	-	+	+	-	+
C63	+	+	+	+	+	+	+	-

The mineral abbreviations are from Whitney and Evans (2010). Symboles (+) and (-) indicate present and absent minerals respectively

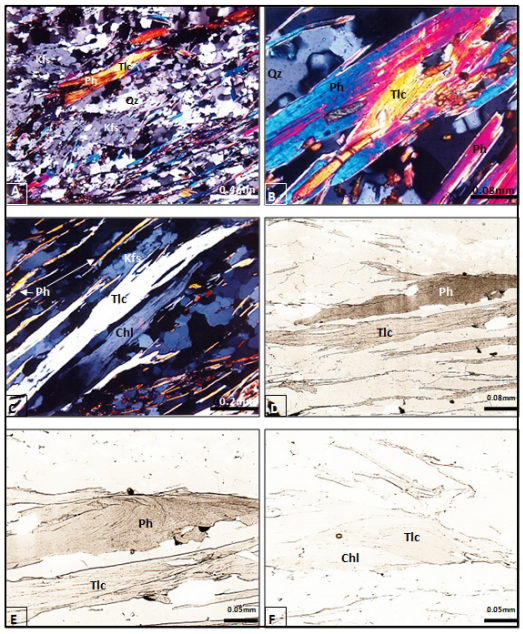

Fig. 4. Photomicrographs of talc-bearing quartz schists showing (A) coexistence of talc, phengite and K-feldspar; (B) intergrowth of talc and phengite; (C) talc, chlorite, phengite and K-feldspar coexistence; (D)-(E) BSE images of coexisting talc and phengite; (F) BSE image of intergrowth of chlorite and talc. Crossed polars. Abbreviations are from Whitney and Evans (2010)

4. Mineral chemistry

Mineral chemistry was acquired by a Cameca SX50 electron microprobe equipped with three wavelength dispersive spectrometers at Toronto University, Canada and a Cameca SX100 at Iran Mineral Processing Research Center (IMPRC). The accelerating voltage and the beam current were maintained at 15 kv and 10 nA, respectively. Corrections were made using either the ZAF or Phi-Rho-Z method following Armstrong (1988). We did not increase the spot size to attempt to minimize the alkali loss, because this would have obscured evidence of any zoning in mica. However, the risk of using mica analyses with a significant contamination or alkali loss was reduced using the method proposed by Vidal and Parra (2000). Unfortunately, in the absence of direct measurement, it is impossible to estimate precisely the Fe^{3+}-content from EPMA. However, it is generally accepted that Fe^{3+} in chlorite group minerals is controlled by crystallochemical constraints rather than fo_2 conditions and is never abundant (Deer et al., 1992; Zane and Sassi, 1998). Therefore, chlorite octahedral contents were calculated from EPMA analyses with the assumption that $Fe^{2+} = Fe^{total}$ could be a real feature. In contrast, Guidotti et al. (1994c) showed that proportion of Fe^{3+} substituting for Al in mica is controlled by fo_2 in which Fe^{3+} is minimal in rocks containing carbonate and graphite. In order to limit the possibility for white micas to contain Fe^{3+}, we preferentially used graphite or at least carbonate-bearing samples. Under such low fo_2 condition the assumption of $Fe^{2+} = Fe^{total}$ was also considered for talc.

4.1. Chlorite

Following the method proposed by Vidal and Parra (2000), only chlorite compositions that could be expressed as a linear combination of amesite, clinochlore, daphnite and sudoite end-members were retained. The distribution of cations on the different sites (Table 2) follows Holland et al. (1998), whereby octahedral Al in clinochlore, daphnite and amesite is restricted to the octahedral M1 and M4 sites with a strong preference for M4, and tetrahedral Al is restricted to T2 on which it substitutes randomly for Si. In addition, we assume that vacancies in sudoite are restricted to the M1 site and that Fe, Mg and Al mix randomly over the (M1+M2) (equal Mg/Fe proportions in these sites). Comparing cation site distributions between chlorite from two assemblages indicates that the chlorite from talc-free assemblage contains higher amounts of $Si_{(T1+T2)}$, $Fe_{(M1)}$, $Al_{(M1)}$, $\square_{(M1)}$ and lesser amounts of $Al_{(T2)}$, $Mg_{(M2+M3)}$, $Fe_{(M2+M3)}$, $Al_{(M2+M3)}$ while $Al_{(M4)}$, $Mg_{(M1)}$ are almost similar (average composition of chlorite from talc-bearing assemblage: $Si_{(T1+T2)} = 2.7$, $Fe_{(M1)} = 0.25$, $Al_{(M1)} = 0.44$, $\square_{(M1)} = 0.2$, $Al_{(T2)} = 1.3$, $Mg_{(M2+M3)} = 1.1$, $Fe_{(M2+M3)} = 2.5$, $Al_{(M2+M3)} = 0.27$, $Al_{(M4)} = 1$, $Mg_{(M1)} = 0.11$; average composition of chlorite from talc-free assemblage: $Si_{(T1+T2)} = 3.01$, $Fe_{(M1)} = 0.32$, $Al_{(M1)} = 0.70$, $\square_{(M1)} = 0.43$, $Al_{(T2)} = 0.98$, $Mg_{(M2+M3)} = 0.87$, $Fe_{(M2+M3)} = 2.25$, $Al_{(M2+M3)} = 0.14$, $Al_{(M4)} = 1$, $Mg_{(M1)}=0.12$) (Table 2). The chlorite compositions of both talc-bearing and talc-free assemblage deviate from the ideal clinochlore composition by Tschermak substitution ($MgSi = Al_{-1}Al_{-1}$) towards amesite, and they also deviate from

the clinochlore composition by Fe^{2+}=Mg substitution towards daphnite (Fig. 5A). Considering Vidal and Parra (2000) diagrams for major substitution, chlorite of the talc-free assemblage contains more amesite and sudoite end-members. The deviation towards sudoite is related to di/trioctahedral substitution (Mg, $Fe^{2+})_3$ = □Al^{-2}) (Fig. 5A).

Table. 2. Representative analyses of chlorites from talc-bearing and talc-free quartz schists

Mineral Asset	Tlc-bearing	Tlc-bearing	Tlc-free	Tlc-free
Point No.	21	23	9	18
SiO_2	24.51	23.18	28.44	28.50
TiO_2	0.06	0.09	0.07	0.02
Al_2O_3	22.61	22.37	22.63	22.71
FeO	28.55	29.40	29.61	28.15
MnO	0.53	0.43	0.38	0.32
MgO	7.17	7.27	6.54	6.07
CaO	0.19	0.09	0.20	0.18
Na_2O	0.18	0.13	0.10	0.06
K_2O	0.57	0.37	1.40	1.62
Total	84.37	88.33	89.37	87.63
Atom site (O=14)				
$Si_{(T1+T2)}$	2.75	2.65	2.99	3.04
$Al_{(T2)}$	1.25	1.35	1.01	0.96
$Al_{(M4)}$	1.00	1.00	1.00	1.00
$Mg_{(M1)}$	0.11	0.11	0.13	0.11
$Fe_{(M1)}$	0.25	0.26	0.33	0.30
$Al_{(M1)}$	0.40	0.47	0.55	0.86
□$_{(M1)}$	0.24	0.16	0.40	0.46
$Mg_{(M2+M3)}$	1.08	1.13	0.90	0.85
$Fe_{(M2+M3)}$	2.43	2.55	2.28	2.22
$Al_{(M2+M3)}$	0.34	0.20	0.25	0.03

Cation site distributions follow Holland et al. (1998). All Fe was considered as FeO following Zane and Sassi (1998) and Guidotti et al. (1994c)

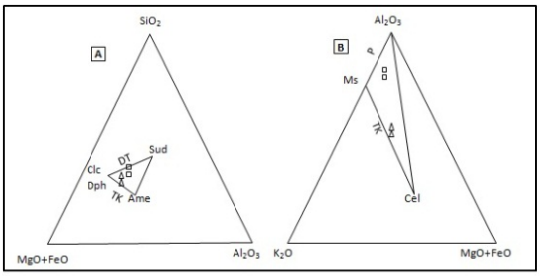

Fig. 5. Relevant substitutions responsible for the compositional variability of chlorites (A) and white micas (B) represented in SMFA and AKMF ternary diagrams. The mineral abbreviations are from Whitney and Evans (2010). TK: Tschermak substitution; DT: di/trioctahedral substitution; P: pyrophyllite substitution; △ : talc-bearing assemblage; □: talc-free assemblage

4.2. White mica

Following the method proposed by Vidal and Parra (2000), only white mica compositions that could be expressed as a linear combination of the celadonite, muscovite, paragonite and pyrophyllite end-members were used. Structural formulae of white micas were calculated from the remaining analyses on a 11-oxygen basis. Six distinct sites can be recognized within the crystal structure of white mica: two tetrahedral $(T1)_2$ and $(T2)_2$, three octahedral (M1), (M2) and (M3), and one interlayer A sites (Parra et al., 2002). The distribution of cations among the different sites is constrained by the following observations: tetrahedral ordering is favored in the 3T structure, for phengitic compositions, and for Si: Al^{IV} ratios near 1:1 (Bailey, 1984). For the other polytypes, refinements did not lead to the detection of any substantial degree of tetrahedral ordering in micas (Bailey, 1984). However, Haselton et al. (1995) suggest that the distribution of Al and Si in tetrahedral sites of 2M1 muscovite is nearly ordered. This indicates short-range Al/Si ordering, at least to the extent of obeying the Al-avoidance role. In the following we assume a partial Si/Al ordering with T1 filled by Si only (Parra et al., 2002). Octahedral cation ordering occurs between cations of different sizes and charges. In particular, Al^{VI} shows a strong preference for M2 and M3 sites, whereas the vacancies and the excess of Fe + Mg cations resulting from the di/trioctahedral substitution are primarily located in the larger M1 octahedrons. The cation site distribution model used here, which stems from the above constraints, is given in Table 3. This model does not differentiate the M2 and M3 sites of similar sizes (collectively referred to as the M2 site of multiplicity 2) (Parra et al., 2002). Comparing cation site distributions between white mica from two assemblages shows that white mica from talc-bearing assemblage contains higher amounts of $Si_{(T1,T2)}$, $Mg_{(M2+M3)}$ and $K_{(A)}$ and lesser amounts of $Al_{(T2)}$, $Al_{(M2+M3)}$ and □$_{(A)}$ than those of talc-free assemblage (average cation site distributions of white mica from talc-bearing assemblage: $Si_{(T1+T2)}$ = 3.3, $Mg_{(M2+M3)}$ = 0.43, $K_{(A)}$ = 0.77, $Al_{(T2)}$ = 0.70, $Al_{(M2+M3)}$ = 1.54, □$_A$ = 0.16; average cation site distributions of white mica from talc-free assemblage: $Si_{(T1+T2)}$ = 2.98, $Mg_{(M2+M3)}$ = 0.03, $K_{(A)}$ = 0.62, $Al_{(T2)}$ = 1.01, $Al_{(M2+M3)}$ = 1.96, □$_A$ = 0.23) (Table 3). By plotting white mica compositions on the Vidal and Parra (2000) diagram for major substitutions in white micas, it is evident that white mica composition from talc-bearing assemblage deviates from ideal muscovite end-member by Tschermak substitution (MgSi = $Al_{-1}Al_{-1}$) towards celadonite and by Mg = Fe^{2+} substitution towards Fe-celadonite (Fig. 5B). But, the white mica from the talc-free assemblage is close to ideal muscovite end-member composition and only deviates towards pyrophyllite by pyrophyllite substitution (KAl = Si_{-1} □) (Fig. 5B).

4.3. Talc

Following Holland and Powell (1998, 1990) four distinct sites have been considered within the crystal structure of talc; two tetrahedral $(T1)_2$ and

$T2)_2$, two octahedral $(M1)_2$ and (M3). The distribution of cations on the different sites (Table 4) follows Wei and Powell (2003), whereby octahedral Al is assumed to order onto the M3 site and tetrahedral Al is restricted to T1 on which it substitutes for Si. The two T2 sites are filled by Si only. Octahedral M3 site is filled by Al^{VI} and Mg + Fe, where as the excess of Mg + Fe and the possible vacancies resulting from di/trioctahedral substitution are located in two M1 octahedrons. The chemical composition of the talc deviates from the ideal talc composition by $Mg = Fe^{2+}$ substitution towards Fe-talc and by $MgSi = Al_{-1}Al_{-1}$ towards Tschermak-talc. A remarkable feature of talc analyses is the high percentage of iron especially in the talc not coexisting with phenigite or chlorite that leads to molar contents of minnesotatite ($Fe_3Si_4O_{10}(OH_2)$). Talc coexisting with phengite or chlorite contains higher amounts of $Mg_{(M3)}$ and $Mg_{(M1)}$ and lesser amount of $Fe_{(M1)}$ ($Mg_{(M3)} = 0.98$, $Mg_{(M1)} = 1.41$ and $Fe_{(M1)} = 0.45$ for talc coexisting with phengite or chlorite and $Mg_{(M3)} = 0.93$, $Mg_{(M1)} = 0.40$ and $Fe_{(M1)} = 1.10$ for talc not coexisting with phengite or chlorite) (Table 4). The relative distribution of Fe-Mg among coexisting phengite, chlorite and talc shows that relative to phengite and talc, chlorite is enriched in Fe-content while distribution coefficient for phengite-talc pair is close to one indicating relatively equal Fe-Mg partitioning between two minerals ($K_D^{Ph\text{-}Chl} = 0.07$, $K_D^{Ph\text{-}Tlc} = 0.93$, $K_D^{Chl\text{-}Tlc} = 12.17$).

Table 3. Representative analyses of white micas from talc-bearing and talc-free quartz schists

Mineral Asset	Tlc-bearing	Tlc-bearing	Tlc-free	Tlc-free
Point No.	17	12	16	25
SiO_2	50.05	50.85	45.27	45.83
TiO_2	0.26	0.14	0.16	0.18
Al_2O_3	29.35	28.92	37.86	39.33
FeO	1.48	1.50	1.29	1.65
MnO	0.27	0.28	0.05	0.07
MgO	4.36	5.12	0.33	0.64
CaO	0.05	0.04	0.04	0.13
Na_2O	0.54	0.62	1.16	1.07
K_2O	9.34	9.21	8.10	6.82
Total	95.70	96.68	94.26	95.72
Atom site (O=11)				
$Si_{(T1+T2)}$	3.29	3.30	3.10	2.97
$Al_{(T2)}$	0.71	0.69	1.00	1.03
$Al_{(M2+M3)}$	1.56	1.52	1.96	1.97
$Mg_{(M2+M3)}$	0.41	0.45	0.05	0.02
$Fe_{(M2+M3)}$	0.02	0.02	0.02	0.009
$Mg_{(M1)}$	0.02	0.05	0.006	0.04
$Fe_{(M1)}$	0.06	0.06	0.004	0.08
$□_{(M1)}$	0.93	0.90	0.94	0.88
$K_{(A)}$	0.78	0.76	0.69	0.56
$Na_{(A)}$	0.07	0.08	0.15	0.13
$□_{(A)}$	0.15	016	0.16	0.30

Cation distributions follow Parra et al. (2002). All Fe was considered as FeO following Guidotti et al. (1994c)

Table 4. Representative analyses of talc

Point No.	7	8	8	6
SiO_2	61.12	61.20	62.32	60.21
TiO_2	0.02	0.07	0.02	0.08
Al_2O_3	0.25	0.30	1.36	0.27
FeO	8.17	8.02	19.22	19.02
MnO	0.05	0.00	0.18	0.00
MgO	23.62	24.98	10.40	15.97
CaO	0.12	0.02	0.30	0.04
Na_2O	0.00	0.00	0.09	0.10
K_2O	0.00	0.00	0.30	0.32
Total	94.19	96.01	94.19	96.01
Atom site (O=11)				
$Si_{(T1+T2)}$	4.00	4.00	4.30	4.11
$Al_{(M3)}$	0.02	0.02	0.11	0.02
$Mg_{(M3)}$	0.98	0.98	0.89	0.98
$Mg_{(M1)}$	1.41	1.46	0.40	0.64
$Fe_{(M1)}$	0.45	0.44	1.11	1.08
$□_{(M1)}$	0.14	0.10	0.75	0.28

Cation site distributions follow Wei and Powell (2003). All Fe was considered as FeO following Guidotti et al. (1994c)

4.4. K-feldspar

EPMA analyses of K-feldspar show that its chemical composition is close to the ideal K-feldspar and is homogeneous (Table 5).

Table 5. Representative analyses of K-feldspars from talc-bearing and talc-free quartz schists

Mineral Asset	Tlc-bearing	Tlc-bearing	Tlc-free	Tlc-free
Point No.	27	28	30	31
SiO_2	65.21	64.71	64.02	65.43
TiO_2	0.16	0.21	0.10	0.05
Al_2O_3	18.62	19.71	19.86	18.11
MgO	0.14	0.06	0.02	0.10
CaO	0.15	0.12	0.14	0.11
Na_2O	0.67	0.98	0.84	0.76
K_2O	14.96	14.13	14.44	14.85
Total	99.92	99.93	99.43	99.42
Atom site (O=8)				
Si	3.00	2.97	2.95	3.00
Ti	0.006	0.007	0.003	0.002
Al	1.00	1.06	1.08	0.98
Mg	0.01	0.004	0.001	0.007
Ca	0.007	0.006	0.007	0.005
Na	0.06	0.09	0.08	0.07
K	0.88	0.83	0.85	0.87
Total	4.96	4.96	4.97	4.96

5. Discussion

Massonne and Schreyer (1989) purely on theoretical grounds in simplified KMASH model system, proposed a high-pressure condition for talc-phengite-K-feldspar assemblage. They suggest that two reactions:

(1) chlorite + phlogopite + quartz = talc + phengite + H_2O

(2) chlorite + K-feldspar = phengite + phlogopite + quartz + H_2O intersect at an invariant point about 11 kbar and around 350°C. The locations of both reactions have been determined experimentally by Massonne and Schreyer (1987, 1989). Thus, the resulting invariant point contains chlorite, K-feldspar, phengite, phlogopite, quartz, talc and H_2O.

From this invariant point, three more reactions could theoretically be obtained. Reaction (3) represents the low-temperature limit of the talc-phengite assemblage:

(3) chlorite + K-feldsper + quartz = talc + phengite + H_2O

The other two are phlogopite + quartz breakdown reactions:

(4) phlogopite + quartz + H_2O = talc + K-feldspar + chlorite

(5) phlogopoite + quartz + H_2O = talc + phengite + K-feldspar

With this configuration, the talc-phengite-K-feldspar assemblage could be stable under high-pressure conditions, whereas the chlorite-K-feldspar-phlogopite is a stable assemblage under low-pressure conditions. However, talc-bearing quartz schists in this study contain significant amount of Fe as well as phases with considerable solid-solutions such as phengite, chlorite and talc. Therefore, the petrogenetic gird proposed by Massonne and Schreyer (1989) cannot be directly applied for the mineral assemblage of the present samples. To consider the P-T stability of talc-phengite-chlorite-K-feldspar assemblage in the studied rocks, a petrogenetic gird was constructed in the K_2O-FeO-MgO-Al_2O_3-SiO_2-H_2O (KFMASH) model system with talc, chlorite, phengite, K-feldspar, phlogopite and kyanite assuming excess quartz and H_2O. We used the internally consistent thermodynamic dataset of Holland and Powell (1998) and the THERMOCALC 3.21 software (Powell et al., 1998). A quaternary symmetric mixing model was adopted for chlorite following Holland et al. (1998). Interaction parameters are W(afchl, clin) = 18 kjmol-1, W(afchl, daph) = 14.5 kjmol-1, W(clin, ames) = 18 kjmol-1 and W(daph, ames) = 13.5kjmol-1. Following Parra et al. (2002) a non-ideal mixing model was used for white mica considering muscovite, celadonite and Fe-celadonite end-members. The interaction margules parameters (W_{Al-Mg} and W_{Al-Fe} at M2 site) were calculated similar to that adopted by Parra et al. (2002) and the intersite interactions of W_{Al-Si} at T2 and W_{Fe-Mg} at M2+M1 were assumed to be zero. For talc, an ideal mixing model was used in which the Al is assumed to order onto the M3 site and to enter only the two T1 sites. Based on Gibbs phase rule, an invariant point for a 6 system component in a P-T field requires that 8 phases be in equilibrium, and a univariant reaction curve requires 7 phases. For the general case, one system with 8 phases (phengite, talc, chlorite, K-feldspar, kyanite, phlogopite, quartz, H_2O) and 6 components (K_2O, FeO, MgO, Al_2O_3, SiO_2, H_2O) contains one invariant point, 6 reaction curves and 15 divariant fields considering quartz and H_2O as excess phases (Fig. 6) (Table 6). In the obtained petrogenetic gird, the divariant field of talc-phengite-chlorite-K-feldspar, comparable with the observed assemblage in talc-bearing quartz schist, is stable over a wide range of P-T condition defined by the following two univariant reactions (Fig. 6).

phengite + talc + quartz = chlorite + K-feldspar + kyanite + H_2O

chlorite + phlogopite + quartz = talc + phengite + K-feldspar + H_2O

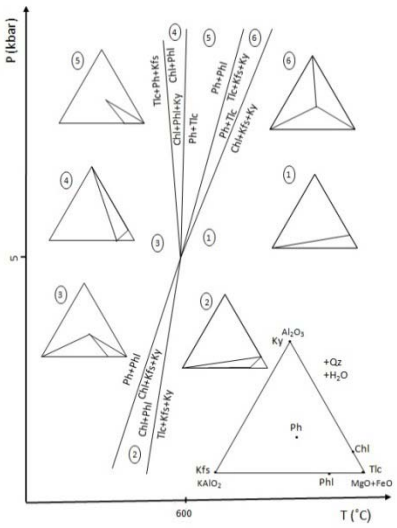

Fig. 6. Petrogenetic grid in the KMASH model system containing chlorite, phengite, K-feldspar, kyanite and phlogopite with excess SiO_2 + H_2O. The mineral abbreviations are from Whitney and Evans (2010)

Table 6. Univariant reactions (A) and divariant assemblages (B) in the KFMASH model system containing phengite, chlorite, talc, kyanite and phlogopite with excess quartz and H_2O

A	
Absent phase	Univariant reactions
[Chl]	Ph + Phl + Qz = Tlc + Kfs + Ky + H2O
[Phl]	Chl + Phl + Qz = Tlc + Kfs + Ky + H2O
[Tlc]	Ph + Phl + Qz = Chl + Kfs + Ky + H2O
[Kfs]	Chl + Ky + Phl + Qz = Ph + Tlc + H2O
[Ky]	Chl + Phl + Qz = Tlc + Ph + Kfs + H2O
[Phl]	Ph + Tlc + Qz = Chl + Kfs + Ky + H2O
B	
Absent phase	Univariant assemblages
[Chl + Ph]	Tlc + Kfs + Ky + Phl
[Chl + Tlc]	Ph + Kfs + Ky + Phl
[Chl + Kfs]	Ph + Tlc + Ky +Phl
[Chl + Ky]	Ph + Tlc + Kfs + Phl
[Chl + Phl]	Ph + Tlc + Kfs + Ky
[Ph + Tlc]	Chl + Kfs + Ky + Phl
[Ph + Kfs]	Chl + Tlc + Ky + Phl
[Ph + Ky]	Chl + Tlc + Kfs + Phl
[Ph + Phl]	Chl + Tlc + Kfs + Ky
[Tlc + Kfs]	Chl + Ph + Ky + Phl
[Tlc + Ky]	Chl + Ph + Kfs + Phl
[Tlc + Phl]	Chl + Ph + Kfs + Ky
[Kfs + Ky]	Chl + Ph + Tlc+ Phl
[Kfs + Phl]	Chl + Ph + Tlc + Ky
[Ky + Phl]	Chl + Ph + Kfs + Tlc

This assemblage is stable above 5 kbar pressure and between 400°C and 800°C. Therefore, to find the certain P-T condition of the observed

assemblage one way is to find a relationship between compositions of talc, phengite and chlorite in different P-T conditions by construction compatibility diagrams. The compatibility diagrams show all phase relationships for all compositions in a defined model system at the specified P-T conditions. To illustrate the changes in the compositions of coexisting minerals with respect to P-T conditions, a series of calculated Al_2O_3-$KAlO_2$-MgO+FeO (AKM) compatibility diagrams with phengite, chlorite and talc were drawn for a traverse from 5 kbar to 11 kbar (Fig. 7). For construction the compatibility diagrams at given P-T points (e.g. 5kbar-400°C, 5kbar- 600°C), the mode 1 (phase diagram calculations) of the THERMOCALC 3.21 software (Powell et al., 1998) and internally consistent thermodynamic dataset of Holland and Powell (1998) were used. In the obtained compatibility diagrams, the compositions of coexisting minerals (phengite, chlorite and talc) have been calculated by the following parameters: X_{Ph} = Fe/Fe+Mg, Y_{Ph} = X(Al, M2A), X_{Chl} = Fe/Fe+Mg, Y_{Chl} = X(Al, T2), X_{Tlc} = Fe/Fe+Mg and Y_{Tlc} = X(Al, M3). In the calculated compatibility diagrams, increasing pressure and temperature, with the exception of phengite composition at P = 11 kbar and T = 400°C, leads to increasing of X_{Ph}, X_{Chl} and X_{Tlc} (for example at P = 5 kbar and T = 400°C: X_{Ph} = 0.473, Y_{Ph} = 0.776, X_{Chl} = 0.163, Y_{Chl} = 0.517, X_{Tlc} = 0.064, Y_{Tlc} = 0.066 but at P = 11 kbar and T = 600°C: X_{Ph} = 0.944, Y_{Ph} = 0.528, X_{Chl} = 0.865, Y_{Chl} = 0.544, X_{Tlc} = 0.750, Y_{Tlc} = 0.130) (Fig. 7). Comparing the compositions of the observed minerals of phengite, chlorite and talc from talc-bearing quartz schists of the Nahavand area with those of calculated compatibility diagrams shows that the greatest similarity can be seen at P = 11 kbar and T = 400°C (compositions of phengite, chlorite and talc from talc-bearing quartz schits: X_{Ph} = 0.280, Y_{Ph} = 0.860, X_{Chl} = 0.570, Y_{Chl} = 0.640, X_{Tlc} = 0.160, Y_{Tlc} = 0.02; compositions of phengite, chlorite and talc shown by compatibility diagram; X_{Ph} = 0.244, Y_{Ph} = 0.828, X_{Chl} = 0.610, Y_{Chl} = 0.644, X_{Tlc} = 0.150, Y_{Tlc} = 0.03) (Fig. 7). Therefore, the observed coexisting minerals of phengite (X_{Ph} = o.280, Y_{Ph} = 0.860), chlorite (X_{Chl} = 0.570, Y_{Chl} = 0.640), talc (X_{Tlc} = 0.160, Y_{Tlc} = 0.020) and K-feldspar are stable at P = 11 kbar and T = 400°C.

The other way to find the relationships between chemical compositions of minerals in equilibrium, is the construction of P-T diagram with the chemical isopleths of coexisting minerals. Because, the Si content in phengite is changing more markedly, it has been used to conclude the pressure of equilibrations at a defined temperature. P-T diagram showing the stability of divariant assemblage of talc-phengite-chlorite-K-feldspar is represented in Fig. 8. Univariant reaction curves restricting the assemblage to the low- and high-T sides are taken from Fig. 6. The Si content of phengite was calculated by the mode 1 of the THERMOCALC 3.21 software (Powell et al., 1998). Considering average Si content of the analysed phengite (Si=3.3) (Table 3), indicate formation pressure of 12 kbar at specified temperature of 580°C which is invariant temperature in Fig. 6.

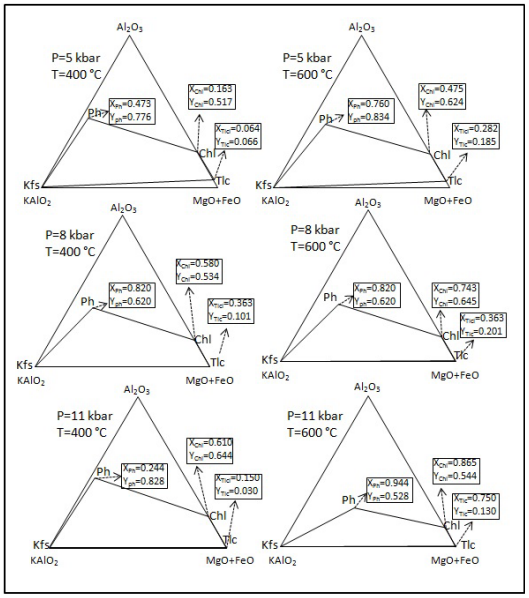

Fig. 7. Calculated Al_2O_3-$KAlO_2$-MgO+FeO (AKM) compatibility diagrams illustrating the changes in the compositions of coexisting minerals of phengite, chlorite and talc with excess quartz and H_2O with respect to P-T conditions. The mineral abbreviations are from Whitney and Evans (2010)

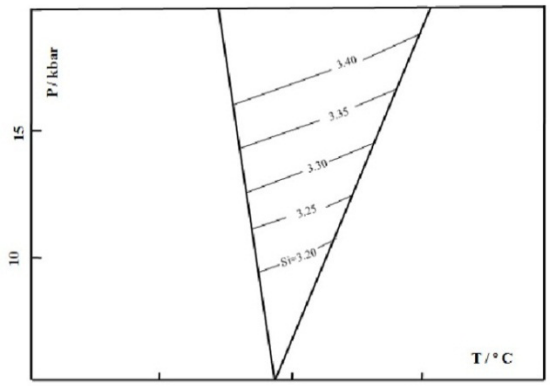

Fig. 8. Calculated P-T diagram with isopleths of Si content in phengite. Univariant curves restricting the assemblage of talc-phengite-chlorite-K-feldspar to the low- and high- T sides are taken from Fig. 6

The relatively high-pressure condition of talc-phengite-chlorite-K-feldspar assemblage in talc-bearing quartz schists from north of the Nahavand

area indicates that this assemblage could be formed during subduction of the Neo-Tethys oceanic plate under the Iranian microcontinent. Such an interpretation is in agreement with Berberian and King (1981), Alavi (1994), Mohajjel et al. (2003), Ghasemi and Talbot (2006) and Dvoudian et al.'s (2007) conclusions.

6. Conclusion

1-For the first time, an unusual assemblage of talc-phengite-chlorite-K-feldspar was found in quartz schists in the Nahavand area from the Sanandaj-Sirjan zone.
2-Based on the field occurrences and mineral assemblages, the quartz schists of the Nahavand region can be divided into talc-bearing and talc-free types.
3-Constructed petrogenetic grid in the KFMASH model system shows that talc-phengite-chlorite-K-feldspar assemblage is stable over a wide range of P-T condition. However the AKM compatibility diagram predicts that phengite (X_{Ph} = 0.280, Y_{Ph} = 0.860), chlorite (X_{Chl} = 0.570, Y_{Chl} = 0.640), talc (X_{Tlc} = 0.160, Y_{Tlc} = 0.02), K-feldspar with excess quartz and H_2O could be stable at P = 11 kbar and T = 400°C.
4-The relatively high-pressure assemblage of talc-phengite-chlorite-K-feldspar could be formed due to the Neo-Tethys oceanic plate subduction under Iranian microcontinent.

Acknowledgements

We are most thankful to the University of Zanjan for the financial support of this study. The authors thank Y. Liou for her help with microprobe analysis.

References

Abraham, K., & Schreyer, W. (1976). A talc-phengite assemblage in piemontite schist from Brezovica, Serbia. Yugoslavia. *Journal of Petrology,* 17, 421-39.

Agard, P., Monié, P., Gerber, W., Omrani, J., Molinaro, M., Meyer, B., Labrousse, L., Vrielynck, B., Jolivet, L., & Yamato, P. (2006). Transient, synobduction exhumation of Zagros blueshists inferred from P-T, deformation, time, and kinematic constraints: Implications for Neotethyan wedge dynamics. *Journal of Geophysical Research,* 111, 1-28.

Alavi, M. (1994). Tectonics of the Zagros orogenic belt of Iran: new data and interpretations. *Tectonophysics,* 229, 211-238.

Alavi, M., & Mahdavi, M. A. (1994). Stratigraphy and structures of the Nahavand region in western Iran, and their implications for the Zagros tectonics. *Geological Magazine,* 131, 43-47.

Armstrong, J. T. (1988). Quantitative analysis of silicates and oxide minerals: comparison of Monte-Carlo, ZAF and Phi-Rho-Z procedure. *Microbeam Analysis*, 239-246.

Bailey, S. W. (1984). Classification and structures of the micas. In: S. W. Bailey (Ed.), *Review in Mineralogy*, 13, 1-12.

Berberian, M., & King, G. C. (1981). Towards a paleogeography and tectonics evolution of Iran. *Canadian Journal of Earth Sciences,* 18, 210-265.

Chopin, C. (1981). Talc-phengite: A widespread assemblage in high-grade pelitic blue schists of the western Alps. *Journal of Petrology,* 22, 628-50.

Davoudian, A. R., Genser, J., Dachs, E., & Shabanian, N. (2007). Petrology of eclogites from north of Shahrekord, Sanandaj-Sirjan Zone, Iran. *Mineralogy and Petrology*, 1-21.

Deer, W. A., Howie, R. A., & Zussman, J. (1992). *An introduction to the rock-forming minerals*. England: Second Edition, Longman Scientific and Technical.

Frank, W., Höck, V., & Miller, C. (1987). Metamorphic and tectonic history of the central Tauern window. In: H. W. Flügel, & P. Faupl (Eds.), *Geodynamics of Eastern Alps (pp. 34-54)*. Deuticke, Vienna.

Ghasemi, A., & Talbot, C. (2006). A new tectonic scenario for the Sanandaj-Sirjan Zone (Iran). *Journal of Asian Earth Sciences,* 26, 683-693.

Guidotti, C. V., Yates, M. G., Dyar, M. D., & Taylor, M. E. (1994c). Petrogenetic significance of the Fe^{3+} content of muscovite in pelitic schists. *American Mineralogist,* 79, 793-795.

Haselton, H. T., Cygan, C. L., & Jenkin, D. M. (1995). Experimental study of muscovite stability in pure H_2O and 1 molal KCl-HCl solutions. *Geochimica et Cosmochimica Acta,* 59, 429-442.

Hatanaka, A., & Hirajima, T. (1999). Talc-forming reaction in piemontite quartz schists of Koutsu area in the Sanbagawa metamorphic belt, eastern Shihkoku. *Abstract Volume for the 106th Annual Meeting of Geological Society of Japan (in Japanese)*, 273.

Holland, T. J. B., & Powell, R. (1998). An internally consistent thermodynamic dataset for phases of petrological interest. *Journal of Metamorphic Geology,* 16, 309-43.

Holland, T. J. B., Baker, J., & Powell, R. (1998). Mixing properties and activity-composition relationships of chlorites in the system $MgO-FeO-Al_2O_3-SiO_2-H_2O$. *European Journal of Mineralogy,* 10, 395-406.

Holland, T. J. B., & Powell, R. (1990). An internally-consistent thermodynamic dataset with uncertainties and correlations: the system $Na_2O-K_2O-CaO-MgO-MnO-FeO-Fe_2O_3-Al_2O_3-SiO_2-TiO_2-C-H_2-O_2$. *Journal of Metamorphic Geology,* 8, 89-124.

Izadyar, J., Hirajima, T., & Nakamura, D. (2000). Talc-phengite-albite assemblage in piemontite-quartz schist of the Sanbagawa metamorphic belt in central Shikoku, Japan. *Island Arc,* 9, 145-58.

Liou, J. G., & Zhang, R. Y. (1995). Significance of ultrahigh-P talc-bearing eclogite assemblages. *Mineralogical Magazine,* 59, 93-102.

Massonne, H., J., & Schreyer, W. (1989). Stability field of the high-pressure assemblages talc-phengite and two new phengite barometers. *European Journal of Mineralogy,* 1, 391-410.

Massonne, H. J., & Schreyer, W. (1987). Phengite geobarometry based on the limiting assemblages with

K-feldspar, phlogopite and quartz. *Contributions to Mineralogy and Petrology,* 96, 212-224.

Mattinson, C. G., Zhang, R. Y., Tsujimori, T., & Liou, J. G. (2004). Epidote-rich talc-kyanite-phengite eclogites, Sulu Terrane, eastern China; P-T-fo_2 estimates and the significance of the epidote-talc assemblage in eclogite. *American Mineralogist,* 89, 1772-83.

Meyre, C., de Capitani, C., Zack, T., & Frey, M. (1999). Petrology of high-pressure metapelites from the Adula Nappe (central Alps, Switzerland). *Journal of Petrology,* 40, 199-213.

Mohajjel, M. Fergusson, C. L., & Sahandi, M. R. (2003). Cretaceous-Tertiary convergence and continental collision, Sanandaj-Sirjan Zone, western Iran. *Journal of Asian Earth Sciences,* 21, 397-412.

Mohajjel, M., & Fergusson, C. L. (2000). Dextral transpression in Late Cretaceous continental collision, Sanandaj-Sirjan Zone, western Iran. *Journal of Structural Geology,* 22, 1125-1139.

Parra, T., Vidal, O., & Agard, P. (2002). A themodynamic model for Fe-Mg dioctahedral K white micas using data from phase-equilibrium experiments and natural pelitic assemblages. *Contributions to Mineralogy and Petrology,* 143, 706-732.

Powell, R., Holland, T. J. B., & Worley, B. (1998). Calculating phase diagrams with THERMOCALC: methods and examples. *Journal of Metamorphic Geology,* 6, 173-204.

Reinecke, T. (1991). Very high-pressure metamorphism and uplift of coesite-bearing metasediments from the Zermatt-Sass zone, western Alps. *European Journal of Mineralogy,* 3, 7-17.

Sengör, A. M. C., & Natalin, B. A. (1996). Paleotectonics of Asia: fragments of a synthesis. In: A. Yin & T. M. Harrison (Eds.), *The tectonic evolution of Asia (pp. 486-640)*. Cambridge: Cambridge University Press.

Sengör, A. M. C. (1984). The cimmeride orogenic system and tectonics of Eurasia. *Geological Society of America Special Paper*, 195.

Stöclin, J. (1968). Structural history and tectonics of Iran: a review. *American Association Petroleum Geology Bulletin,* 52, 1229-1258.

Theye, T., Seidel, E., & Vidal, O. (1992). Carpholite, sudoite and chloritoid in low-grade high-pressure metapelites from Crete and the Peloponnese, Greece. *European Journal of Mineralogy,* 4, 487-507.

Ubukawa, T., Hatanaka, A., Matsumoto, K., & Hirajima, T. (2007). Pseudosection analysis for talc-Na pyroxene-bearing piemontite-quartz schist in the Sanbagawa Belt, Japan. *Island Arc,* 16, 553-574.

Vidal, O., & Parra, T. (2000). Exhumation paths of high-pressure metapelites obtained from local equilibria for chlorite-phengite assemblages. *Geological Journal,* 35, 139-161.

Wei, C., & Powell, R. (2003). Phase relations in high-pressure metapelites in the system KFMASH(K_2O-FeO-Al_2O_3-SiO_2-H_2O) with application to natural rocks. *Contributions to Mineralogy and Petrology*, 145, 301-315.

Wei, C., & Powell, R. (2004). Calculated phase relations in high-pressure metapelites in the system NKFMASH (Na_2O-K_2O-FeO-MgO-Al_2O_3-SiO_2-H_2O). *Journal of Petrology,* 45, 183-202.

Whitney, D., & Evans, B. W. (2010). Abbreviations for names of rock-forming minerals. *American Mineralogist,* 95, 185-187.

Zane A., & Sassi, R. (1998). New data on metamorphic chlorite as a petrogenetic indicator mineral, with special regard to greenschist-facies rocks. *Canadian Mineralogist,* 36, 713-726.